Informatics in Medicine Unlocked 15 (2019) 100155

Contents lists available at ScienceDirect

Informatics in Medicine Unlocked

journal homepage: www.elsevier.com/locate/imu

A novel approach to estimate the upper limb reaching movement in three-dimensional space

Luigi Iuppariello[a], Giovanni D'addio[b,*], Bernardo Lanzillo[c], Piero Balbi[c], Emilio Andreozzi[a,b], Giovanni Improta[d], Giuliana Faiella[a], Mario Cesarelli[a,b]

[a] Department of Electric Engineering and Information Technologies (DIETI), School of Engineering, University of Naples Federico II, Naples, Italy
[b] Bioengineering Department, Istituti Clinici Scientifici Maugeri SpA Società Benefit, IRCCS Telese Terme, Benevento, Italy
[c] Neurology Department- Istituti Clinici Scientifici Maugeri SpA Società Benefit, IRCCS Telese Terme, Benevento, Italy
[d] Department of Public Health (DSP), School of Medicine and Surgery, University of Naples Federico II, Naples, Italy

ARTICLE INFO

Keywords:
Reaching movements
Minimum jerk model
Reaching movements
Rehabilitation

ABSTRACT

Background: In spite of the complexity that the number of redundancy levels suggests, humans show amazingly regularities when generating movement. When moving the hand between pairs of targets, subjects tended to generate roughly straight hand trajectories with single-peaked, bell-shaped speed profiles. The original minimum-jerk model, in which limb displacement is represented by a fifth order polynomial, has been shown to predict qualitative features of experimental trajectories recorded in monkeys performing intermediate speed one-joint elbow movements to a target. However, it is difficult to compare a real (experimentally measured) movement to its equivalent minimum-jerk trajectory (MJT) because the exact start and end times and positions of real movements are usually not well defined: even discrete movements usually exhibit an extended period of low (but non-zero) velocity and acceleration before and after a movement, making estimation of the exact start and end times inaccurate.

Aim: The purpose of this study was to describe a method used for correctly fitting the minimum jerk trajectory to real movement data assuming that the minimum-jerk trajectory satisfies the same threshold condition as the real movement (the same position and the same percentage of maximum velocity), rather than the movements start and end at full rest. Thus, the original minimum-jerk model was revised.

Materials and methods: Starting from the original minimum-jerk model, in this work is proposed a method used for correctly fitting the minimum jerk trajectory to real movement data defined by a threshold condition. This method enables users to accurately compare a minimum-jerk trajectory to real movements. The latter were recorded using APDM inertial sensors. To estimate if the ideal model fits adequately the real reaching movements we consider three kinematic indexes.

Results: and Discussion: A total of 100 upper arm straight line reaching movements executed by healthy subjects were acquired. MJTs follow closely to the reaching movements when they have been computed considering the revised model. On the contrary, the MJTs do not follow the real profiles when considering the original formulation. This behaviour is confirmed when we consider the three kinematic indexes. These findings help us better understand important characteristics of movements in health. Future works will focus on the investigation of the performance of the upper arm straight line reaching movements in a larger healthy subjects sample and then in pathological conditions.

1. Introduction

Human arm motor control has been a subject of investigation for several decades, during which some issues have been identified as themes of high interest [1]. Among these are problems such as planning, execution and learning. In a broad sense, the motor control problem can be stated as the generation of the muscle activations that best fit the purpose of a movement or manipulation task, given the proprioceptive and external world information available through the body sensors. The organizing principle of the motion is an ill-posed problem, in mathematical parlance. Even in a simple task such as reaching a target in free space, a multitude of possible solutions are

* Corresponding author.
E-mail address: gianni.daddio@icsmaugeri.it (G. D'addio).

https://doi.org/10.1016/j.imu.2019.01.005
Received 25 October 2018; Received in revised form 12 January 2019; Accepted 27 January 2019
Available online 11 March 2019

available, each one being a path that takes the hand from the initial to the final position. Infinite solutions exist not only for this path but also for the velocity profile used to track it. The freedom to choose both the path and the velocity profile defines the underlying redundancy in a movement task. However, redundancy arises not only in the nature of movement tasks but also as an intrinsic and beneficial feature of the human body, which provides for more flexibility to carry out complex tasks. One aspect of this redundancy results from the 7° of freedom (DOF) of the kinematic structure of the human arm (3 at the shoulder, 2 at the elbow, and 2 at the wrist), which exceeds the minimum necessary number (6 DOF) to move the hand in the three-dimensional space [1]. In spite of the complexity that the number of redundancy levels suggests, humans show amazingly regularities when generating movement. One of the most robust results, which has been observed [2–13], is the characteristic segmentation of the hand velocity profile and the coupling between shape and speed of the trajectories. When moving the hand between pairs of targets, subjects tended to generate roughly straight hand trajectories with single-peaked, bell-shaped speed profiles; this behaviour was independent of the part of the work-space in which the movement was performed. In 1984 [14] Hogan presented a model in which the reproduction of bell-shaped profiles was a main concern. Since natural movements tend to be characteristically *smooth* and graceful, he suggested that among all possible trajectories, the one that produces maximum smoothness is most likely to be selected. Mathematically, smoothness measure has been based on minimizing jerk, the first-time derivative of acceleration. This has been formalized by using dynamic optimization theory to determine the *movement*, which minimizes the rate of change of acceleration (jerk) of the limb, thus, *the unique trajectory which yields the best performance*. The conclusion was that the maximization of smoothness for a motion, between start and end point, may be modelled by minimizing the mean-square jerk. The minimum-jerk model, in which limb displacement is represented by a fifth order polynomial, has been shown to predict qualitative features of experimental trajectories recorded in monkeys performing intermediate speed one-joint elbow movements to a target. The model has been further generalized to planar two-joint arm movements with some success in qualitatively and quantitatively fitting certain features of those movements [15]. The minimum-jerk model predicted symmetric, bell-shaped velocity profiles and assumed that movements started and ended at full rest.

However, it is difficult to compare a real (experimentally measured) movement to its equivalent minimum-jerk trajectory (MJT) because the exact start and end times and positions of real movements are usually not well defined: even discrete movements usually exhibit an extended period of low (but non-zero) velocity and acceleration before and after a movement, making estimation of the exact start and end times inaccurate.

For this reason, taking inspiration from a previous study [16], the start and end of real movements are here defined through a threshold condition, such as when the speed exceeds a percentage (5%) of the peak speed. Because the equation for the MJT assumes different boundary conditions (zero speed and acceleration at the start and end) than the threshold condition, fitting a MJT to real movement data defined by a threshold condition results in an incorrect fit.

So, starting from the original minimum-jerk model, in this work is proposed a method used for correctly fitting the minimum jerk trajectory to real movement data defined by a threshold condition. This method enables users to accurately fit (and therefore compare) a minimum-jerk trajectory to real movements. Moreover, in order to underline the differences between the two formulations for the MJTs, we fit the real movements with the obtained MJTs with the minimum jerk model proposed by Flash and Hogan, For the movement recording we used inertial sensors, so this work also proposes the extension of such model in the three-dimensional space. To the best of our knowledge, no study investigates a revised minimum-jerk trajectory for the upper limb reaching movements recorded with inertial sensors in the three-dimensional space.

2. Materials and methods

2.1. The original minimum jerk formulation

Hogan [14] has proposed a principle underlying the selection of a movement trajectory by the central nervous system (CNS). He suggested that among all possible trajectories, the one that produces maximum smoothness is most likely to be selected. Mathematically, he chose as a measure of smoothness, minimization of the integral of mean squared jerk (the third time derivative of displacement). The minimum jerk model has been formalized by using dynamic optimization theory to determine the movement, which minimizes the rate of change of acceleration (jerk) of the limb, thus, the unique trajectory which yields the best performance. Briefly, the optimization's technique in Cartesian coordinates (x and y), on the plane, was introduced by Flash and Hogan in 1985 [15]. It requires the definition of a criterion function, C, that has to be minimized:

$$C = \int_0^d \frac{\gamma^2}{2} dt = \frac{1}{2}\int_0^d \left(\left(\frac{d^3x}{dt^3}\right)^2 + \left(\frac{d^3y}{dt^3}\right)^2\right)dt \tag{1}$$

C is the criterion function, usually called objective function, t is time, d is duration of movement, and γ denotes jerk. The form of the minimum – jerk movement trajectory x(t) and y(t) are expressed by a fifth order polynomial in time, defined considering a sufficient set of boundary condition, as follows:

$$x(t) = x_0 + (x_f - x_0)(15\tau^4 - 6\tau^5 - 10\tau^3) \tag{2}$$

$$y(t) = y_0 + (y_f - y_0)(15\tau^4 - 6\tau^5 - 10\tau^3) \tag{3}$$

where $\tau = t/t_f$, x_0, y_0, are the initial hand position coordinates at t = 0, and x_f, y_f are the final hand position coordinates at $t = t_f$.

In Appendix A, the dynamic optimization theory proposed by Hogan, for planar reaching movements, is explained in detail.

2.2. The new minimum jerk model in the 3D space: the problem formulation

The original formulation of the minimum jerk model assumes movements that start and end at full rest. However, a real movement usually exhibits an extended period of low (but non-null) velocity and acceleration before and after the true movement, making estimation of the exact start and end time points inaccurate. We decided to consider and fit only the central part of the movement where the velocity is higher than a prefixed threshold usually set to 5% or 10% of the peak speed. In this way, the obtained MJT better fits the real movement. A real movement trajectory (RMT) trough three-dimensional space is given by $x_{tot}(t) = [x(t), y(t), z(t)]^T$, where t and T represent time and the transpose operator, respectively. We consider this trajectory defined over the interval $t_1 \le t \le t_2$ where t_1 and t_2 are defined by the following conditions [16]:

$$\|\dot{x}_{tot}(t_1)\| = \alpha \|\dot{x}_{tot}\|_{max} \tag{4}$$

$$\|\dot{x}_{tot}(t_2)\| = \alpha \|\dot{x}_{tot}\|_{max} \tag{5}$$

where $\|\dot{x}_{tot}(t)\| = \sqrt{[\dot{x}(t)]^2 + [\dot{y}(t)]^2 + [\dot{z}(t)]^2}$ is the speed of the trajectory at time t, $\|\dot{x}_{tot}\|_{max}$ is the maximum speed between t_1 and t_2, and t is a proportional constant (often 5%), $x_{tot}(t)$ represents a single real movement.

To better adapt the MJT ($\hat{x}(t)_{tot}$) to the real movement ($x_{tot}(t)$), we consider the MJT which assumes, at t_1 and t_2 time, the same position and the same percentage of the peak velocity of the real movement according to the following equations:

$$\hat{x}(t_1)_{tot} = x_{tot}(t_1) \tag{6}$$

$$\hat{x}(t_2)_{tot} = x_{tot}(t_2) \tag{7}$$

$$\|\dot{\hat{x}}(t_1)_{tot}\| = \alpha\|\dot{x}(t)_{tot}\|_{max} \tag{8}$$

$$\|\dot{\hat{x}}(t_2)_{tot}\| = \alpha\|\dot{\hat{x}}(t)_{tot}\|_{max} \tag{9}$$

2.3. The new minimum jerk model in the 3D space: the problem solution

The MJT proposed by Flash and Hogan is given as:

$$x_{tot}(t) = x_{tot}(t_i) + [x_{tot}(t_f) - x_{tot}(t_i)]\left[10\left(\frac{t-t_i}{d}\right)^3 - 15\left(\frac{t-t_i}{d}\right)^4 + 6\left(\frac{t-t_i}{d}\right)^5\right] \tag{10}$$

where $\hat{x}(t)_{tot} = [\hat{x}(t), \hat{y}(t), \hat{z}(t)]$ is defined over the $t_i \le t \le t_f$ and t is the movement duration defined as

$d = t_f - t_i$.

Therefore, the task of finding $\hat{x}(t)_{tot}$ reduces to identifying t_i, t_f,. For a real movement trajectory (RMT) we can only estimate the time instants t_1 and t_2, applying conditions (1.8) and (1.9), and compute the corresponding positions on the trajectory. However, in order to utilize the expression (1.10) we should compute the time instants t_i and t_f and the corresponding positions $\hat{x}(t_i)_{tot}, \hat{x}(t_f)_{tot}$. To apply conditions (1.8) and (1.9), it needs to identify in advance the maximum speed for the proposed model. In appendix B we demonstrate that the maximum speed in the MJT can be expressed as:

$$\|\dot{\hat{x}}(t)_{tot}\|_{max} = \frac{30}{16}\frac{\|\hat{x}(t_f)_{tot} - \hat{x}(t_i)_{tot}\|}{d} = \frac{15}{8}\frac{\|\hat{x}(t_f)_{tot} - \hat{x}(t_i)_{tot}\|}{d} \tag{11}$$

Applying the conditions (or constrains) (1.8) and (1.9) considering the previous expression of maximum velocity we can individuate the time instants t_1 and t_2. After that, we compute the expression for the trajectory positions in the time instants t_1 and t_2 and place them equal to the value of the real movement trajectory

$\hat{x}(t_1)_{tot} = x_{tot}(t_1),\ \hat{x}(t_2)_{tot} = x_{tot}(t_2),$

In this way we can compute the values of trajectory position $\hat{x}(t_i)_{tot}$, $\hat{x}(t_f)_{tot}$ and the t_i, t_f time to substitute into equation (B.7) obtaining the desired MJT, as reported in appendix B.

2.4. Compatibility between real and ideal trajectories

To estimate if the ideal model fits adequately the real reaching movements we consider three kinematic indexes computed on both the RMT and MJT. In this contest, they can be considered as performance indexes, defined as follows:

- *Level of Smoothness (SL)*,
- *Arm Path Ratio (APR),*
- *Mean Distance (MD).*

The SL is related to the original concept of the smooth movements proposed by Hogan. The quality of the movement is evaluated introducing the kinematic index ***Level of Smoothness (SL)*** defined as follows:

$$SL = \frac{J_m - J_i}{J_m}$$

J_m is the normalized smoothness (NS) measured on the subject's reaching movement (or real reaching movement) while J_i is the NS obtained considering the ideal movement extracted by the minimum jerk theory. The smoothness of the movement is evaluated computing the jerk cost functional defined as:

$$J = \frac{1}{2}\int_{t_1}^{t_2}\left(\left(\frac{d^3x(t)}{dt^3}\right)^2 + \left(\frac{d^3y(t)}{dt^3}\right)^2 + \left(\frac{d^3z(t)}{dt^3}\right)^2\right)dt$$

where t_1 and t_2 have been defined in the previous paragraph. Jerk is the rate of the change of acceleration with respect to time (third time derivative of the position). To test the hypothesis that movements to different targets and/or of different duration were simply scaled replicas of a standard movement, normalized smoothness (NS) is considered:

$$J = \frac{1}{2}\left\{\int_{t_1}^{t_2}\left[\left(\frac{d^3x}{dt^3}\right)^2 + \left(\frac{d^3y}{dt^3}\right)^2 + \left(\frac{d^3z}{dt^3}\right)^2\right]dt\right\}\frac{d^5}{A^2}$$

where A is the movement amplitude and $d = t_2 - t_1$, its duration.

The Arm Path Ratio parameter considers the hand's trajectory. Comparing the ideal trajectory described by the MJT with the real trajectory. You can assess the difference between the real straight line reaching movement and ideal straight line reaching movement. You have to calculate the area covered by the velocity curve respect to time in two abovementioned cases.

$$APR = \frac{Area_{\mathrm{Real-Velocity}}}{Area_{Ideal-Velocity}}$$

An Arm path ratio near to 1 indicates a good performance.

The Mean Distance represents the mean value of the absolute distance between each point of the real trajectory and that predicted by the minimum jerk model:

$$MD = \frac{\sum_{i=1}^{n}|d_i|}{n}$$

Values around zero indicate a great accuracy of the movement.

2.5. Acquisition of real movement

In this study was used the APDM movement monitoring solutions, a Wearable Motion Analysis System (WMAS) that provides Inertial Measurements Units (IMU) to collect real reaching movements. The Opal sensor by APDM [17] consists of a tri-axial accelerometer, tri-axial gyroscope and tri-axial magnetometer. The accelerometer, gyroscope, and magnetometer are all encased into a small unit of 48.4 × 36.1 × 13.4 mm (L x W x H) and weighs less than 22 g. One major benefit of the Opal sensor is it can collect data for an entire day (up to 16 h) on one charge and store up to 28 days' worth of data. About Sensor Characteristics the accelerometer range is ± 2 g or ± 6 g. This is approximately equal to ± 20 or ± 60 m/s^2, although some sensors may have a slightly larger range before saturating. The APDM instrumentation includes a laptop, Motion Studio software, docking station, access point, two USB cables, an external power adapter, several Opal IMUs, and for each sensor two small Velcro straps. To assess the straight-line reaching movement, one IMU is located near the wrist. We collect 100 straight lines reaching movements in the three-dimensional space performed by 12 healthy subjects (six men, 35-45 years-old; six females, 30–50 years old). They have been clearly informed regarding the nature of the study, the timetable, possible risks and the informed consent has been obtained from each of them prior to their participation in the study. The movement begins when the hand is near the trunk, case (a). Then the straight line reaching movement continues in the sagittal plane, case (b), and it finishes when the arm reaches its maximum extension, case(c).

2.6. Inertial measures: signal processing

The output of the accelerometers is the measured signal and it is characterized by:

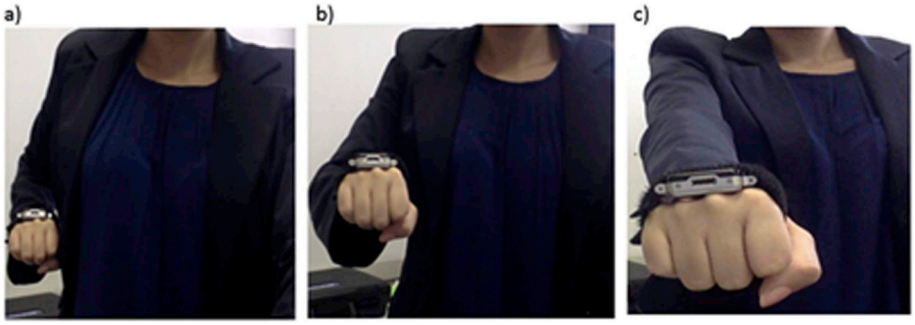

Fig. 1. Straight line reaching movement (healthy subject) The movement begins when the hand is near the trunk, case (a). Then the straight-line reaching movement continues in the sagittal plane, case (b), and it finishes when the arm reaches its maximum extension, case (c).

$$\textit{acquired acceleration} = \textit{inertial acceleration} + \textit{gravity acceleration} + \textit{noise} + \textit{offset}$$

To analyze the reaching movements, we are interested in evaluation only of the inertial acceleration because by means of an inverse kinematics approach, with it, we can deter main the velocity and spatial movements. To do this, it has been considered the subsequent workflow (Fig. 2):

The entire procedure is described in Appendix C and the representation of a typical Inertial Acceleration signal in shown in Fig. 11.

If we compare the acceleration signals in Fig. 7 with the acceleration signals in Fig. 11, we see immediately that z acceleration in Fig. 7 was around 9,8 m/s^2 while in Fig. 11, after the removal of the gravity acceleration, it is around 0 m/s^2.

3. Results

A total of 100 upper arm straight line reaching movements executed by 12 healthy subjects (six men, 35-45 years-old; six females, 30–50 years old) were acquired using IMU sensors, of which 15 recordings

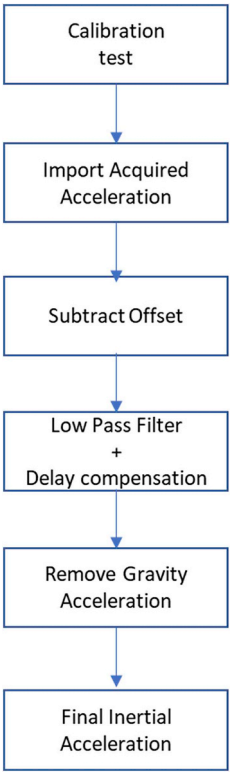

Fig. 2. Workflow of the activities.

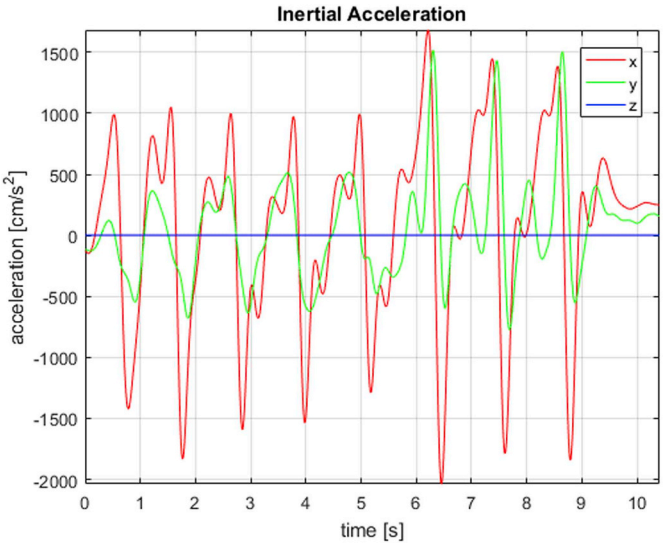

Fig. 11. Inertial Acceleration.

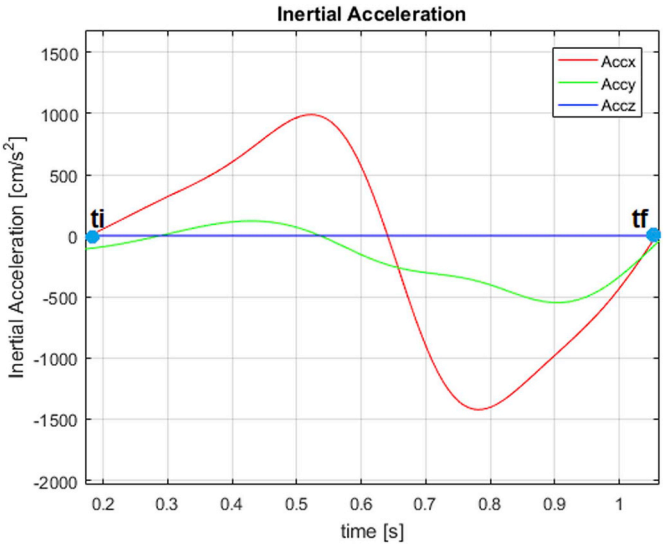

Fig. 12. Inertial acceleration [cm/s^2] of a straight-line movement (t_i is the start time, t_f is the end time).

then were discarded from results due to incorrect tasks performed.

As explained, we acquire the acceleration and trough the signal processing we obtain the inertial acceleration (Fig.12). Then, for our aims, we want to get the velocity and the path space, which are the integration of the acceleration in time and the integration of the

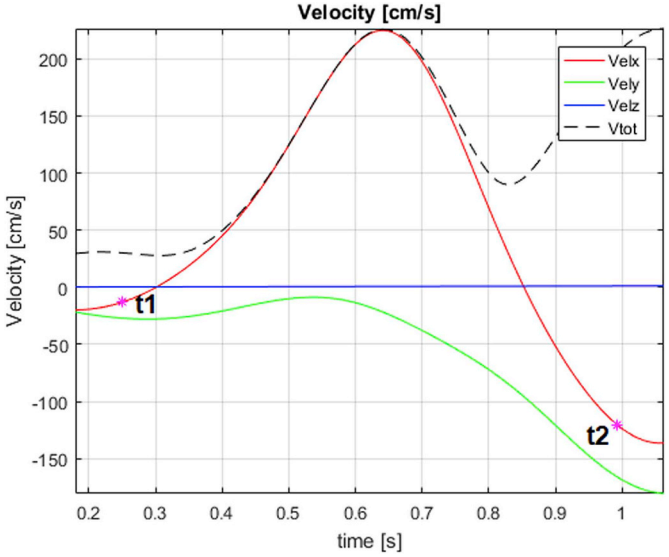

Fig. 13. Velocity profile [cm/s] of a straight-line movement, t_i is the start time and t_f is the end time.

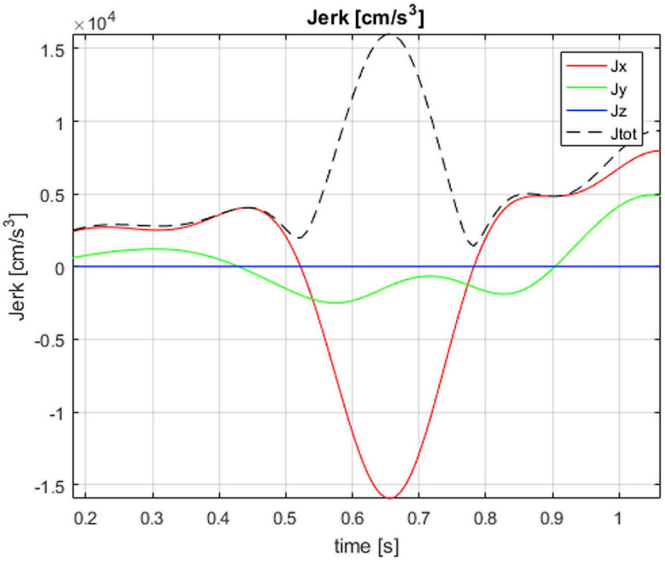

Fig. 15. Jerk's representation [cm/s^3].

velocity in time. So, we compute the cumulative trapezoidal numerical integration. The movement begins at time t_i, when the hand is near the trunk, you can see it in Fig. 6, on the right, case (a). Then the straight line reaching movement continues in the sagittal plane, case (b), and it finishes at time t_f when the arm reaches its maximum extension, case (c).

We integrated the three components of the inertial acceleration, each of them respect to the time, and then we evaluated the Vtot (shown in Fig.13 with dashed line), total velocity, it's equal to:

$$V_{tot} = \sqrt{v_x^2 + v_y^2 + v_z^2}$$

Blue circles represent the moments the subject starts and ends the movement. Red circles represent the approximated beginning and end times (t1 and t2) of the movement, which were determined by the 5% of the maximum speed criteria.

Iterating the same calculus, but considering the three components of velocity as input, we get the real movement trajectory (Fig.14), RMT:

$$RMT = \sqrt{m_x^2 + m_y^2 + m_z^2}$$

Where m indicates the displacement.

Further, the time derivative of the acceleration (Fig.15) has been computed by using ***Savitzky-Golay filter***, a Smoothing and Differentiation Filter, that optimally fits a set of data points to polynomials of different degrees. In our case, we have fixed a polynomial order equal to 3, and a frame length of 19 (chosen empirically).

Finally, both the revised and the original Hogan's formulation have been used to fit the real movements with their equivalent MJTs. In Fig.16 we compare the real (experimentally measured) movement, in

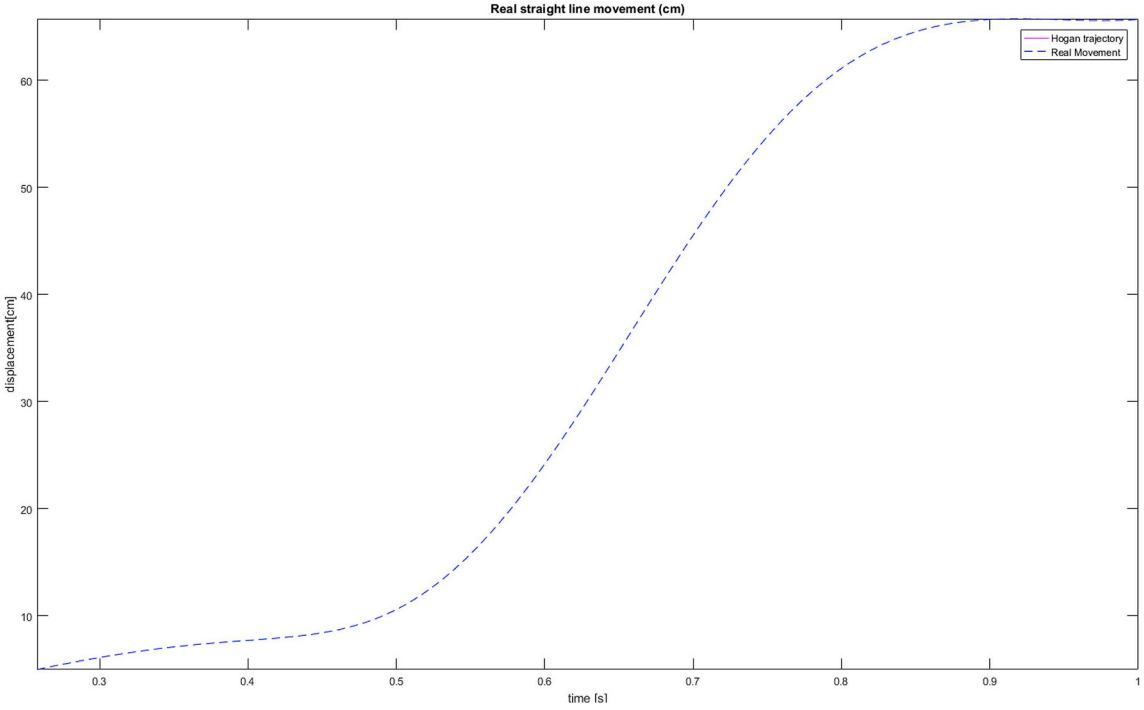

Fig. 14. Real movement trajectory [cm] for straight line reaching movements.

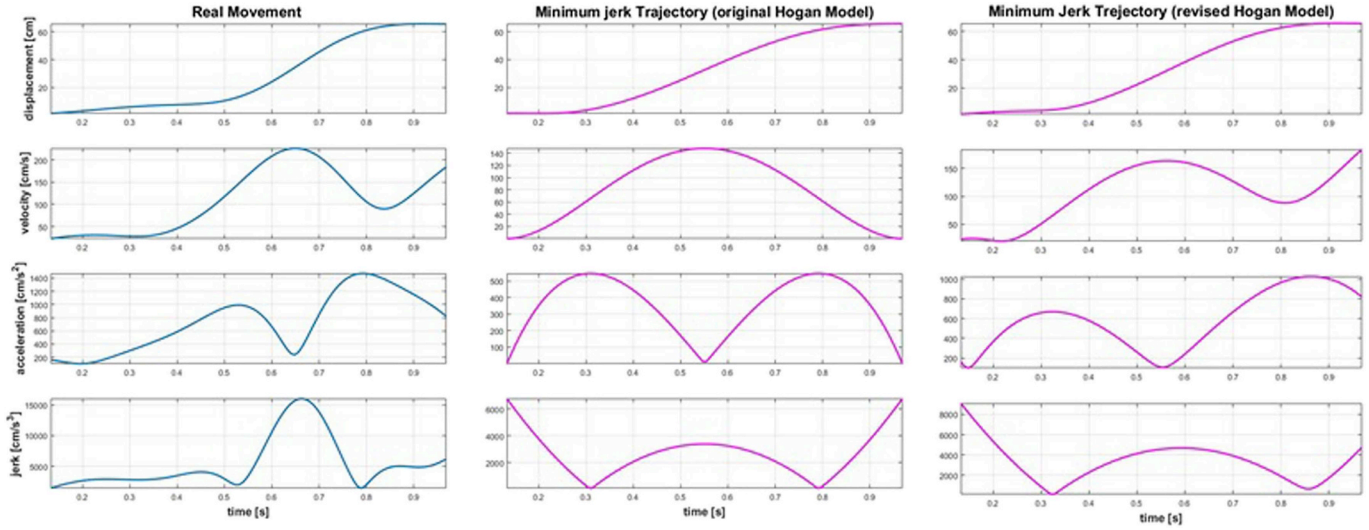

Fig. 16. The displacement [cm], velocity[cm/s], acceleration[cm/sˆ2] and jerk[cm/sˆ3] profiles, in blue for the real straight-line reaching movement and in magenta for the ideal movement defined with both the original and revised Hogan model. On the x-axis are reported the time [s]. (For interpretation of the references to colour in this figure legend, the reader is referred to the Web version of this article.)

blue, to its equivalent MJT, in magenta, defined with both the original and revised Hogan model.

Table 1 reports the kinematic indexes used to assess the quality of reaching movement, computed considering both the revised and original Hogan model.

In order that the ideal model fit adequately the real reaching movements, the values of the SL are around zero, those of the APR are around one and those of the MD are around zero, in the case of healthy subjects.

Considering the mathematical formulation of the kinematic indexes (see materials and methods section – paragraph D), they better describe the accuracy of real movements performed by healthy subjects. In particular, the values of each index are close enough to those computed considering the revised Hogan model. On the contrary, these indexes depart from the expected values when they have been computed with the original Hogan model.

4. Discussion

The reaching movement has been analyzed for more than 100 years. The kinematic study can provide.

accurate and objective information about motor strategies associated with goal-oriented tasks, and monitor administration of therapeutic techniques for the upper extremity.

The minimum-jerk model predicted symmetric, bell-shaped velocity profiles for reaching movements which start and end at full rest [21–25]. However, it is difficult to compare a real (experimentally measured) movement to its equivalent minimum-jerk trajectory (MJT) because the exact start and end times and positions of real movements are usually not well defined: even discrete movements usually exhibit an extended period of low (but non-zero) velocity and acceleration before and after a movement, making estimation of the exact start and end times inaccurate. The purpose of this study was to describe a method used for correctly fitting the minimum jerk trajectory to real movement data, collected using Inertial Measurements Units (IMU), assuming that the minimum-jerk trajectory satisfies the same threshold condition as the real movement (the same position and the same percentage of maximum velocity), rather than the movements start and end at full rest. We extracted real movements from filtered inertial acceleration in three-dimensional space, starting from several straight-line reaching movements performed by healthy subjects. Then, we defined both the revised and the original minimum jerk trajectories (MJT) for each real reaching movement.

Table 1
Kinematic indexes used to assess the quality of reaching movement, computed considering both the revised and original Hogan model.

	Revised Hogan Model	Original Hogan Model
Smoothness Level (SL)	0,44 ± 0,18	0.98 ± 0.21
Arm Path Ratio (APR)	1,00 ± 0,10	1.38 ± 0.50
Mean Distance (MD)	0,97 ± 0,59	5,5 ± 1,00

This study showed interesting results. In fact, MJTs follow closely to the reaching movements when they have been computed considering the revised Hogan model [26–28]. On the contrary, the MJTs do not follow the real profiles when considering the original Hogan formulation [29]. This behaviour is confirmed when we consider the three kinematic indexes computed on both the real data and MJT, in order to evaluate if the ideal model fits adequately the real reaching movements.

In fact, considering the mathematical formulation of the kinematic indexes (see materials and methods section – paragraph D), they better describe the accuracy of real movements performed by healthy subjects: the values of the SL are around zero, the values of the APR are around one and the values of the MD are around zero. On the contrary, these indexes depart from the expected values when they have been computed with the original Hogan model, suggesting the inadequacy of the original Hogan model to correctly describe real movements, when the hypothesis of full rest at the start and at the end of the movements fails.

The compatibility obtained between real measurements and ideal kinematic results computed with the revised Hogan model, allowed us to introduce quantitative parameters and to correctly estimate the performance of upper arm straight line reaching movements, with them. These findings can help us better understand important characteristics of movements in health. A correct understanding of motor strategies for reaching movement in healthy subjects can provide accurate and objective information about motor strategies associated with goal-oriented tasks, when pathological conditions occur. Quantitative measures of human movement quality are significant in the rehabilitation field for expressing the outcomes during rehabilitation treatments and assessing their efficacy [30,31], discriminating between healthy and pathological conditions [32,33], and for helping in the decision making in the clinical setting. Moreover, since controlling the movement of the arm to achieve a goal, such as reaching for an object, requires coordinating many muscles acting on many joints, following

studies will address the analysis of Surface Electromyography for detecting the EMG patterns during reaching or grasping movements (i.e. acceleration and deceleration phases), by using temporal and frequency methods [34–41]. This study modelled a method used for correctly fitting the minimum jerk trajectory to real movement data in free space assuming that the minimum-jerk trajectory satisfies the same threshold condition as the real movement, thus revising the original minimum-jerk model. To the best of our knowledge, no previous studies have been conducted with such aim. However, the following studies will aim to extend the analysis to a larger sample of healthy subjects in order to perform a robust statistical analysis for validating these preliminary results. Subsequently, the it will be possible to investigate the performance of the upper arm straight line reaching movements in pathological conditions, using the above described revised minimum jerk model.

Acknowledgments

This research was partially supported by Bioengineering Department, Istituti Clinici Scientifici Maugeri SpA Società Benefit, IRCCS Telese Terme, Benevento, Italy. We thank the colleagues who provided insight and expertise that greatly assisted the research.

APPENDIX A

The smoothness with which movements are customarily performed has led Hogan [14] to formulate a model for trajectory planning by the central nervous system (CNS) in which the goal is to maximize smoothness. He suggested, thanks to experimental trajectories recorded in monkeys, that among all possible trajectories, the one that produces maximum smoothness is represented by a fifth order polynomial:

$$x(t) = c_0 + c_1 t + c_2 t^2 + c_3 t^3 + c_4 t^4 + c_5 t^5 \tag{A.1}$$

It was assumed as boundary conditions at the onset and termination of the movement, the follow conditions:

$$\begin{cases} x(0) = x_i(initial - position) \\ \dot{x}(0) = V_0 = 0 \\ \ddot{x}(0) = A_0 = 0 \end{cases} \quad \text{(Initial conditions at start time t= 0)}$$

$$\begin{cases} x(T) = D(initial - position) \\ \dot{x}(T) = V_f = 0 \\ \ddot{x}(T) = A_f = 0 \end{cases} \quad \text{(Target conditions at final time t= T)}$$

Movements start and end with zero velocity and acceleration, however given the duration of the straight line reaching movements, the authors defined univocally the trajectory by means of these passages:

$$\dot{x}(t) = c_1 + 2c_2 t + 3c_3 t^2 + 4c_4 t^3 + 5c_5 t^4 \tag{A.2}$$

$$\ddot{x}(t) = 2c_2 + 6c_3 t + 12c_4 t^2 + 20c_5 t^3 \tag{A.3}$$

Applying initial condition with $x_i = 0$:

$$x(0) = c_0 = 0 => \ c_0 = 0$$

$$\dot{x}(0) = c_1 = V_0 = > \ c_1 = V_0$$

$$\ddot{x}(0) = 2c_2 = A_0 = > \ c_2 = A_0/2$$

We obtain $\begin{cases} x(t) = V_0 t + \frac{A_0}{2} t^2 + c_3 t^3 + c_4 t^4 + c_5 t^5 \\ \dot{x}(t) = V_0 + A_0 t + 3c_3 t^2 + 4c_4 t^3 + 5c_5 t^4 \\ \ddot{x}(t) = A_0 + 6c_3 t + 12c_4 t^2 + 20c_5 t^3 \end{cases}$

For target conditions at t = T:

$$\begin{cases} x(t) = V_0 T + \frac{A_0}{2} T^2 + c_3 T^3 + c_4 T^4 + c_5 T^5 = D \\ \dot{x}(t) = V_0 + A_0 T + 3c_3 T^2 + 4c_4 T^3 + 5c_5 T^4 = V_f \rightarrow \\ \ddot{x}(t) = A_0 + 6c_3 T + 12c_4 T^2 + 20c_5 T^3 = A_f \end{cases}$$

$$\begin{cases} c_3 = \frac{D}{T^3} - \left(\frac{V_0}{T^2} + \frac{A_0}{2T} + c_4 T + c_5 T^2\right) \\ c_4 = \frac{V_f}{T^3} - \left(-2\frac{V_0}{T^3} - \frac{1}{2}\frac{A_0}{T^2} + \frac{3D}{T^4} + 2c_5 T\right) \Rightarrow \\ c_5 = \frac{A_f}{2T^3} - \frac{A_0}{2T^3} + 6\frac{D}{T^5} - 3\frac{V_0}{T^4} - 3\frac{V_f}{T^4} \end{cases} \begin{cases} c_3 = 10\frac{D}{T^3} - 6\frac{V_0}{T^4} - \frac{3}{2}\frac{A_0}{T} - 4\frac{V_f}{T^2} + \frac{A_f}{2T} \\ c_4 = \frac{3}{2}\frac{A_0}{T^2} - \frac{A_f}{T^2} + 7\frac{V_f}{T^3} + 8\frac{V_0}{T^3} - 15\frac{D}{T^4} \\ c_5 = \frac{A_f}{2T^3} - \frac{A_0}{2T^3} + 6\frac{D}{T^5} - 3\frac{V_0}{T^4} - 3\frac{V_f}{T^4} \end{cases}$$

Writing the values of c_0, c_1, c_2, c_3, c_4, c_5 in A.1 we get:

$$x(t) = V_0 t + \frac{A_0}{2} t^2 + 10\frac{D}{T^3} t^3 - 6\frac{V_0}{T^4} t^3 - \frac{3}{2}\frac{A_0}{T} t^3 - 4\frac{V_f}{T^2} t^3 + \frac{A_f}{2T} t^3 + \frac{3}{2}\frac{A_0}{T^2} t^4 - \frac{A_f}{T^2} t^4 + 7\frac{V_f}{T^3} t^4 + \ldots$$
$$\ldots + 8\frac{V_0}{T^3} t^4 - 15\frac{D}{T^4} t^4 + \frac{A_f}{2T^3} t^5 - \frac{A_0}{2T^3} t^5 + 6\frac{D}{T^5} t^5 - 3\frac{V_0}{T^4} t^5 - 3\frac{V_f}{T^4} t^5 \tag{A.4}$$

Remembering that $V_0 = V_f = A_0 = A_f = 0$ the equality (1–4) becomes the desired trajectory:

$$x(t) = 10\frac{D}{T^3}t^3 - 15\frac{D}{T^4}t^4 + 6\frac{D}{T^5}t^5 = D\left[10\frac{t^3}{T^3} - 15\frac{t^4}{T^4} + 6\frac{t^5}{T^5}\right] \tag{A.5}$$

APPENDIX B

The original statement of the minimum jerk model assumes movements that start and end at full rest. However, it is difficult to compare a real (experimentally measured) movement to its equivalent MJT (Minimum-Jerk-Trajectory), because even discrete movements usually exhibit an extended period of low (but non-null) velocity and acceleration before and after a movement, making estimation of the exact start and end times inaccurate. Here we describe a method for correctly fitting a MJT to real free space movements More specifically, the start and the end of real movements are estimated considering the 5% or 10% of the peak speed.

Then, we derive the time and position at the start and end of the MJT that satisfies the same threshold condition as the real movement (same position and same percentage of maximum speed). This method enables users to accurately fit (and therefore compare) a MJT to a real movement.

A real movement trajectory (RMT) trough three-dimensional space. This trajectory is given by $x_{tot}(t) = [x(t), y(t), z(t)]^{T}$, where t and T represent time and the transpose operator, respectively. We consider this trajectory defined over the interval $t_1 \le t \le t_2$ and the following conditions [16]:

$$\|\dot{x}_{tot}(t_1)\| = \|\alpha\dot{x}_{tot}\|_{max} \tag{B.1}$$

$$\|\dot{x}_{tot}(t_2)\| = \alpha\|\dot{x}_{tot}\|_{max} \tag{B.2}$$

where $\|\dot{x}_{tot}(t)\| = \sqrt{[\dot{x}(t)]^2 + [\dot{y}(t)]^2 + [\dot{z}(t)]^2}$ is the speed of the trajectory at time t, $\|\dot{x}_{tot}\|_{max}$ is the maximum speed between t_1 and t_2, and α is a proportional constant (often 5%), $x_{tot}(t)$ represents a single movement, the boundary conditions (1.4) and (1.5) permit to find t_1 and t_2.

The problem treats with the prediction of the MJT $\hat{x}(t)_{tot}$ that fits the real movement trajectory $x_{tot}(t)$. The $\hat{x}(t)_{tot}$ is said to fit $x_{tot}(t)$ if they share the same position and proportion of their respective peak speeds at t_1 and t_2:

$$\hat{x}(t_1)_{tot} = x_{tot}(t_1) \tag{B.3}$$

$$\hat{x}(t_2)_{tot} = x_{tot}(t_2) \tag{B.4}$$

$$\|\dot{\hat{x}}(t_1)_{tot}\| = \alpha\|\dot{\hat{x}}(t)_{tot}\|_{max} \tag{B.5}$$

$$\|\dot{\hat{x}}(t_2)_{tot}\| = \alpha\|\dot{\hat{x}}(t)_{tot}\|_{max} \tag{B.6}$$

The MJT proposed by Flash and Hogan (1985) is given as:

$$x_{tot}(t) = x_{tot}(t_i) + [x_{tot}(t_f) - x_{tot}(t_i)]\left[10\left(\frac{t-t_i}{d}\right)^3 - 15\left(\frac{t-t_i}{d}\right)^4 + 6\left(\frac{t-t_i}{d}\right)^5\right] \tag{B.7}$$

where $\hat{x}(t)_{tot} = [\hat{x}(t), \hat{y}(t), \hat{z}(t)]$ is defined over the $t_i \le t \le t_f$ and d is the movement duration defined as $d = t_f - t_i$.

Therefore, the task of finding $\hat{x}(t)_{tot}$ reduces to identifying t_i, t_f, $\hat{x}(t_i)_{tot}$ *and* $\hat{x}(t_f)_{tot}$. Times t_i and t_f can be found from conditions (1.8) and (1.9) as follows. First, the speed of the MJT is derived from velocity

$$\dot{\hat{x}}(t) = \frac{30[\hat{x}(t_f) - \hat{x}(t_i)]}{d}\left[\left(\frac{t-t_i}{d}\right)^2 - 2\left(\frac{t-t_i}{d}\right)^3 + \left(\frac{t-t_i}{d}\right)^4\right] \tag{B.8}$$

$$\|\dot{\hat{x}}_{tot}(t)\| = \frac{30[\hat{x}_{tot}(t_f) - \hat{x}_{tot}(t_i)]}{d}\left[\left(\frac{t-t_i}{d}\right)^2 - 2\left(\frac{t-t_i}{d}\right)^3 + \left(\frac{t-t_i}{d}\right)^4\right] \tag{B.9}$$

where

$$\|\hat{x}_{tot}(t_f) - \hat{x}_{tot}(t_i)\| = \sqrt{[\hat{x}(t_f) - \hat{x}(t_i)]^2 + [\hat{y}(t_f) - \hat{y}(t_i)]^2 + [\hat{z}(t_f) - \hat{z}(t_i)]^2} \tag{B.10}$$

The maximum speed can be found by setting the time derivative of speed equal to zero. There is a maximum when $\left(\frac{t-t_i}{d}\right) = \frac{1}{2}$

Evaluating equation (3) at this normalized time yields

$$\dot{\hat{x}}(t)_{tot\ max} = \frac{30}{16}\frac{\widehat{x}(t_f)_{tot} - \widehat{x}(t_i)_{tot}}{d} = \frac{15}{8}\frac{\widehat{x}(t_f)_{tot} - ,\widehat{x}(t_i)_{tot}}{d} \tag{B.11}$$

Considering 1.8, it results:

$$\|\dot{\hat{x}}_{tot}(t_1)\| = \frac{30\hat{x}_{tot}(t_f) - \hat{x}_{tot}(t_i)}{d}\left[\left(\frac{t_1-t_i}{d}\right)^2 - 2\left(\frac{t_1-t_i}{d}\right)^3 + \left(\frac{t_1-t_i}{d}\right)^4\right] = \alpha\frac{15}{8}\frac{\hat{x}_{tot}(t_f) - \hat{x}_{tot}(t_i)}{d}$$

$$\Rightarrow \frac{30\|\hat{x}_{tot}(t_f) - \hat{x}_{tot}(t_i)\|}{d}\left[\left(\frac{t_1-t_i}{d}\right)^2 - 2\left(\frac{t_1-t_i}{d}\right)^3 + \left(\frac{t_1-t_i}{d}\right)^4 - \frac{\alpha}{16}\right] = 0$$

assuming that

$$\hat{x}(t_f) \neq \hat{x}(t_i) \Rightarrow \left[\left(\frac{t_1-t_i}{d}\right)^2 - 2\left(\frac{t_1-t_i}{d}\right)^3 + \left(\frac{t_1-t_i}{d}\right)^4 - \frac{\alpha}{16}\right] = 0 \tag{B.12}$$

Similarly, for condition 1.9 it results:

$$\left[\left(\frac{t_2-t_i}{d}\right)^2-2\left(\frac{t_2-t_i}{d}\right)^3+\left(\frac{t_2-t_i}{d}\right)^4-\frac{\alpha}{16}\right]=0 \tag{B.13}$$

Substituting $u_1=\left(\frac{t_1-t_i}{d}\right)$ and $u_2=\left(\frac{t_2-t_i}{d}\right)$ into equation (B.17) and B.18 yields

$$u^4{}_{1,2}-2u^3{}_{1,2}+u^2{}_{1,2}-\frac{\alpha}{16}=0 \tag{B.14}$$

We solved equation (B.15) numerically for t = 0,05, obtaining:

$$u^4{}_{1,2}-2u^3{}_{1,2}+u^2{}_{1,2}-\frac{1}{320}=0 \tag{B.15}$$

$$u^2{}_{1,2}(u^2{}_{1,2}-2u_{1,2}+1)=\frac{1}{320} \tag{B.16}$$

$$u^2{}_{1,2}(u_{1,2}-1)^2=\frac{1}{320} \tag{B.17}$$

$$u_{1,2}(u_{1,2}-1)=\pm\sqrt{\frac{1}{320}} \tag{B.18}$$

$$\begin{gathered} u^2{}_{1,2}-u_{1,2}-\sqrt{\tfrac{1}{320}}=0 \\ \Downarrow \\ \Rightarrow\quad u_{1,2}=\tfrac{1\pm\sqrt{1+0{,}223606}}{2} \\ \Downarrow \\ 1)u_{1,2,1}=1{,}053083 \\ 2)u_{1,2,2}=-0{,}053083 \end{gathered} \tag{B.19}$$

$$\begin{gathered} u^2{}_{1,2}-u_{1,2}+\sqrt{\tfrac{1}{320}}=0 \\ \Downarrow \\ u_{1,2}=\tfrac{1\pm\sqrt{1-0{,}223606}}{2} \\ \Downarrow \\ 3)u_{1,2,3}=0{,}940566=u_2 \\ 4)u_{1,2,4}=0{,}059434=u_1 \end{gathered} \tag{B.20}$$

We consider only the solutions 3) and 4) because we have to respect three conditions:
(1)$0<u_1<1$, (2)$0<u_2<1$, and. (3)$u_2>u_1$

There are (1) and (2) because $t_i<t_1<t_2<t_f$ so $u_1=\left(\frac{t_1-t_i}{d}\right)$ and $u_2=\left(\frac{t_2-t_i}{d}\right)$ are two proper fractions lower than 1, major than 0 for physic reasons. The third condition there is because $t_2>t_1$.

Considering the definitions of u_1, u_2, it results

$$t_i=\frac{u_2t_1-u_1t_2}{u_2-u_1} \tag{B.21}$$

$$d=\frac{t_2-t_1}{u_2-u_1} \tag{B.22}$$

$$t_f=t_i+d \tag{B.23}$$

The solutions for $\hat{x}(t_i)_{tot}$ *and* $\hat{x}(t_f)_{tot}$ can be found from 1.6 to 1.7 which require

$$\hat{x}(t_1)_{tot}=x_{tot}(t_1)$$

$$\hat{x}(t_2)_{tot}=x_{tot}(t_2)$$

So

$$\hat{x}(t_1)_{tot}=\ \hat{x}(t_i)+[\hat{x}(t_f)-\hat{x}(t_i)]\left[10\left(\frac{t_1-t_i}{d}\right)^3-15\left(\frac{t_1-t_i}{d}\right)^4+6\left(\frac{t_1-t_i}{d}\right)^5\right]\ =x_{tot}(t_1) \tag{B.24}$$

and

$$\hat{x}(t_2)_{tot}=\ \hat{x}(t_i)+[\hat{x}(t_f)-\hat{x}(t_i)]\left[10\left(\frac{t_2-t_i}{d}\right)^3-15\left(\frac{t_2-t_i}{d}\right)^4+6\left(\frac{t_2-t_i}{d}\right)^5\right]\ =x_{tot}(t_2) \tag{B.25}$$

The expressions for u_1 and u_2 yield to.

$t_1-t_i=u_1d$
$t_2-t_i=u_2d$,

So, the 1.34 and 1.35 reduce to the following system

$$\hat{x}(t_i)_{tot}(1-\gamma_1) + \hat{x}(t_f)_{tot}\gamma_1 = x_{tot}(t_1) \tag{B.26}$$

$$\hat{x}(t_i)_{tot}(1-\gamma_2) + \hat{x}(t_f)_{tot}\gamma_2 = x_{tot}(t_2) \tag{B.27}$$

where γ_1 and γ_2

$$\gamma_1 = 10u_1^3 - 15u_1^4 + 6u_1^5 \tag{B.28}$$

$$\gamma_2 = 10u_2^3 - 15u_2^4 + 6u_2^5 \tag{B.29}$$

solving the system yields

$$\hat{x}(t_i)_{tot} = \frac{v_2 x(t_1) - v_1 x(t_2)}{v_2 - v_1} \tag{B.30}$$

$$\hat{x}(t_f)_{tot} = \frac{(1-v_1)x(t_2) - (1-v_2)x(t_1)}{v_2 - v_1} \tag{B.31}$$

Substituting the values $u_1 = 0.0594$ and $u_2 = 0.9405$ in 1.38 and 1.39 yields $\gamma_1 = 0.0019$ and $\gamma_2 = 0.998$. Since the very small value for γ_1, it can be considered negligible, while γ_2 can be set to 1. This way, 1.32 and 1.34 reduce to

$$\hat{x}(t_i)_{tot} = x_{tot}(t_1)$$

$$\hat{x}(t_f)_{tot} = x_{tot}(t_2)$$

Finally, substituting $\hat{x}(t_i)_{tot}$ and $\hat{x}(t_f)_{tot}$ and the values for t_i and t_f (from equations B.21 and B.23) into equation (B.7) yields the desired MJT.

APPENDIX C

Calibration and offset evaluation

To perform reliable upper-limb kinematics measurements, static calibration and the offset subtraction of the accelerometers has been assessed in the step 1). The monitors come pre-calibrated from APDM. Each monitor is calibrated individually in a procedure that determines optimal scaling factors and offsets for the accelerometers, gyroscopes, and magnetometers across a wide range of orientations and temperatures. While the factory calibration is optimal at the time of shipping, all low power sensors like the ones used in APDM's monitors are subject to small changes over time and may require re-calibration. The re-calibration is performed recording, with the motion studio software, the sensor output for each axis (x, y, z) when it is precisely aligned to the axis of the gravitational acceleration (Fig. 3). After positioning the sensors in the desired position, it needed to wait for 15 s, and the acceleration values recorder were 9,81 m/s^2 (gravity acceleration).

This time represents the warm-up time and it's recommended by the manufacturer.

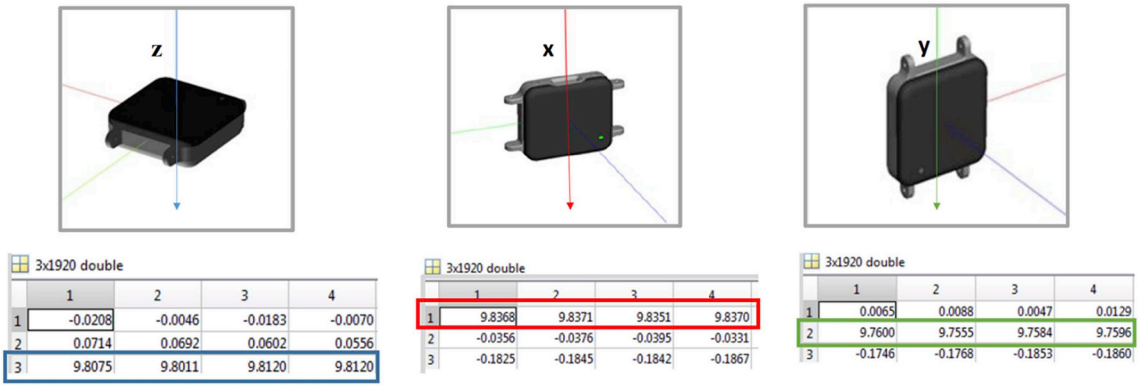

Fig. 3. Accelerometer positioned with the z, x, y axis along the vertical, respectively.

Since Opal IMU sensor includes a triaxial accelerometer, a triaxial gyroscope and a triaxial magnetometer, the sensor output could be sensitive to mutual interference among the three axes. So, for a complete static calibration test the accelerometer has been collocated in tilted manner (Fig. 4) for example with an angle of 45° with respect to the horizontal plane and the total acceleration is assessed according to the following vector summation:

$$Acc_{tot} = \sqrt{ax^2 + ay^2 + az^2}$$

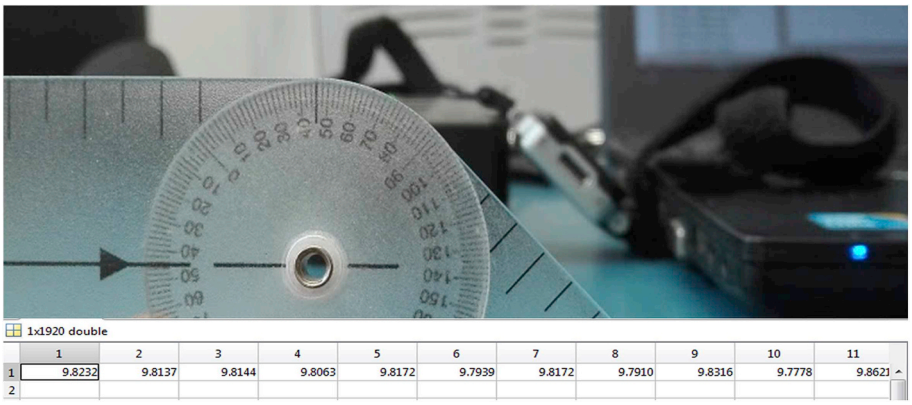

Fig. 4. Acceleration values acquired with the accelerometer in tilted manner.

In all the static trails position, the acceleration value along the vertical axis and the acceleration total value (accelerometer in tilted manner) results as 9.81 m/s^2, so indicating a correct calibration. The static trials position shown in Fig. 1 have been also useful to assess the offset along the axes in the horizontal plane, which values have to be in theory equal to 0. For each axis in the horizontal plane, offsets have been estimated as in the equation below:

$$\Delta Offset = \frac{a_{x+} + a_{x-}}{2}$$

Where a_(x+) and a_(x-) are the signals acquired in static trials positioning the sensor for both faces on a horizontal plane (Fig. 5). Similarly, it is calculated for the y and z axes.

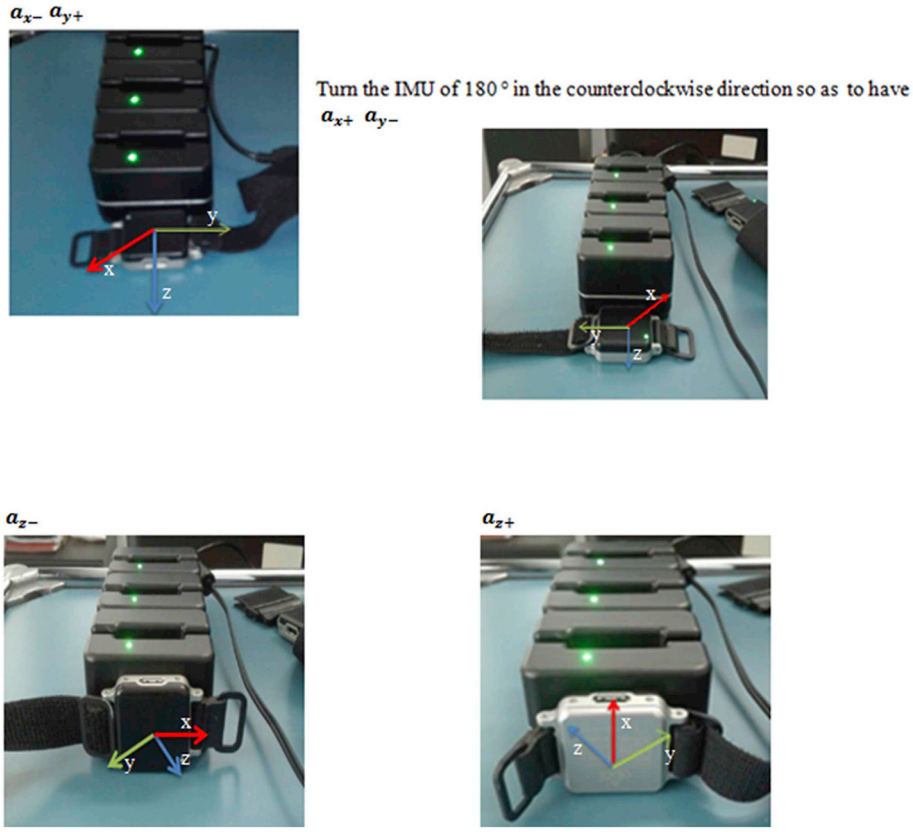

Fig. 5. Offset evaluation. The offset values will be subtracted from the acquired acceleration in a generic time.

Experimental measures

The movement begins at time t_i, when the hand is near the trunk, you can see it in Fig. 6, on the right, case (a). Then the straight line reaching movement continues in the sagittal plane, case (b), and it finishes at time t_f when the arm reaches its maximum extension, case (c).

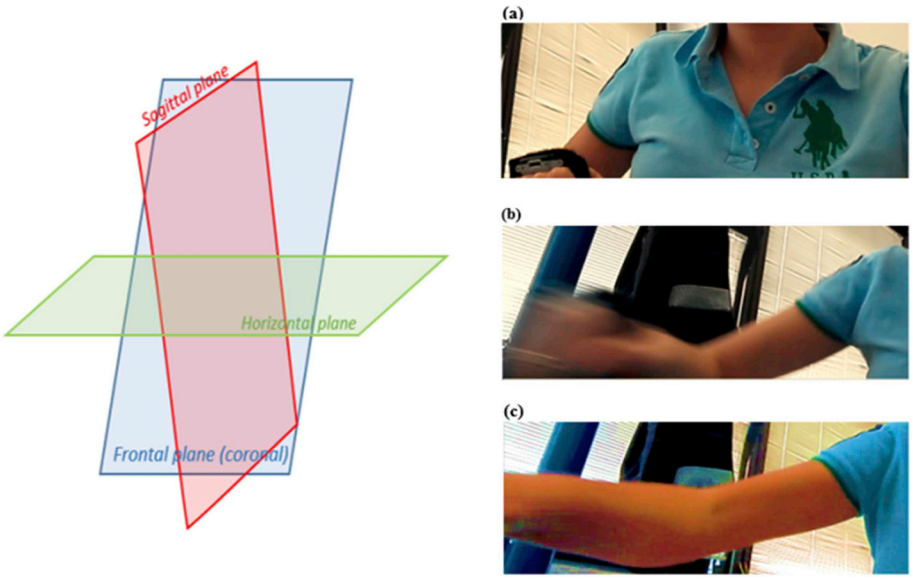

Fig. 6. Execution of a straight line reaching movement. On the left, there are the anatomical planes: Horizontal plane, Frontal plane, Sagittal plane. On the right, the movement begins at time t_i, when the hand is near the trunk, case (a). Then the straight line reaching movement continues in the sagittal plane, case (b), and it finishes at time t_f when the arm reaches its maximum extension, case (c). The sensor output, after performing the above described straight line reaching movements, is shown in Fig. 7.

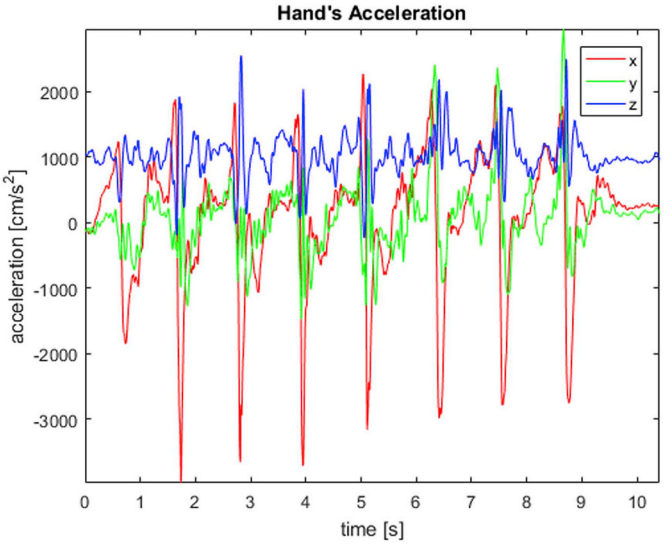

Fig. 7. Hand's Acceleration.

Offset subtraction

In this phase the Offset values have to be removed because as above explained, in static condition and in the horizontal plane we observed acceleration's values which are around zero but not perfectly equal to zero. So:

$ax = ax - xoff$;

$ay = ay - yoff$;

$az = az - zoff$;

Where ax, ay, az are the components of the acceleration signal, xoff, yoff, zoff are the offset along the x, y and z axes, respectively.

Low pass filtering and Delay compensation

As shown in Fig. 7, Acquired Acceleration signal is sensitive to disturbances, it's jagged and not very smooth. In the next step we will apply a low pass filter to the signal to filter on unwanted higher frequencies components. So it has been used a low-pass IIR Butterworth type filter with a cut-off frequency of 3Hz. Choosing the cutoff frequency near 3Hz will preserve the information content in the signal and at the same time smooth the signal.

Finally, a “zero-phase filtering”, filtering the signal in the forward and backward directions, is used to compensate for the delays introduced by such filter. The results of the filtering operation is shown in Fig. 8.

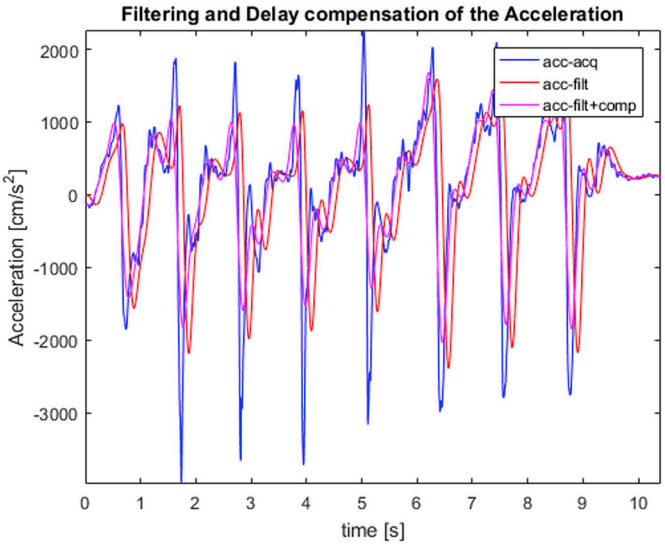

Fig. 8. Filtered Acceleration.

Removal of the gravity acceleration

Get at this point, the measured acceleration is composed by the vector sum of the true vertical and true horizontal components, but for the reaching movements only horizontal acceleration was of interest (Fig. 9). Thus, acquired acceleration of a constantly tilted triaxial accelerometer can be expressed by the following trigonometric relation [18].

$$x_a = x_A \cos a + \sin a \qquad \text{C.1}$$

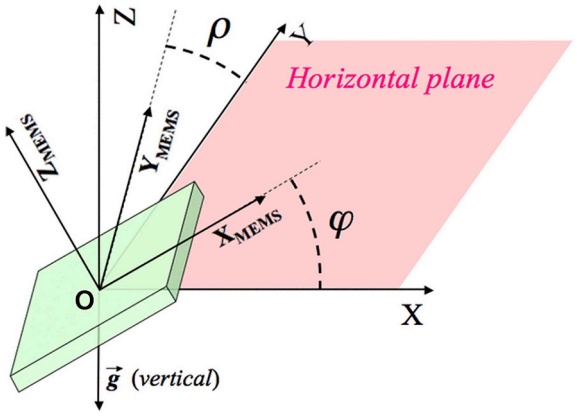

Fig. 9. Measured Acceleration x_a (tilting angle "α", horizontal acceleration factor "$x_A \cos a$ ", gravity component "$\sin \alpha$").

$$x_A = \frac{x_a - \sin a}{\cos a} \qquad \text{C.2}$$

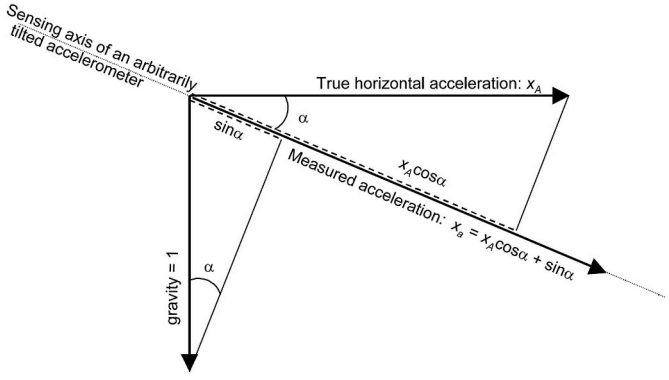

Fig. 10. Angles ϕ and ρ that describe the orientation of the MEMS accelerometer with respect to an absolute reference system having the Z-axis oriented [Autocalibration of MEMS Accelerometers].

We first observe that the orientation of MEMS (Micro Electro Mechanical System) in 3-D space can be defined by only two angles, which

represent the orientation of the device with respect to the gravity vector g; the rotation around an axis parallel to g cannot be observed since the sensor output is invariant for rotations around such an axis. Let us indicate as (φ, ρ) the angles between the XMEMS and YMEMS axes and the horizontal plane Figure 10 [19]. According to Equations C.1, C.2 we can estimate, in equations C.3, C.4, C.5 true x, y, z accelerations that respectively we decide to call APtrueACC (Antero-Posterior true acceleration), MLtrueACC (Medium-Lateral true acceleration), VtrueACC (Vertical true acceleration) [20].

$$APtrueACC = \frac{APACCr - \sin\varphi}{\cos\varphi} \quad \text{C.3}$$

$$MLtrueACC = \frac{MLACCr - \sin\rho}{\cos\rho} \quad \text{C.4}$$

$$VtrueACC = 1 - \sin\varphi - \sin\rho \quad \text{C.5}$$

Where APACCr, MLACCr are static signals, obtained filtering acquired x, y acceleration by means of Butterworth filter with a cut-off frequency of 0,1 Hz and an order equal to 3. The angles ϕ and ρ could be computed considering the following equations:

$$\varphi = \arcsin(APACCr) \quad \text{C.6}$$

$$\rho = \arcsin(MLACCr) \quad \text{C.7}$$

equations C.6 and C.7 are frequently used with biaxial accelerometers, but they suffer from a critical drawback. The sensitivity on the estimated value of φ and ρ depends on the value of φ and ρ itself. To overcome this problem, the following trigonometric equations are used here to compute φ and ρ:

$$\varphi = \arctan\left(\frac{APACCr}{\sqrt{MLACCr^2 + VACCr^2}}\right) \quad \text{C.8}$$

$$\rho = \arctan\left(\frac{MLACCr}{\sqrt{APACCr^2 + VACCr^2}}\right) \quad \text{C.9}$$

These equations guarantee that the accuracy is almost constant inside the whole range of values that φ and ρ can assume [19].

Conflicts of interest

None declared.

Funding

This research received no specific grant from any funding agency in the public, commercial, or not-for-profit sectors.

References

[1] Guigon E, Baraduc P, Desmurget M. Computational motor control: redundancy and invariance. J Neurophysiol 2007;97:331–47. https://doi.org/10.1152/jn.00290.2006.
[2] Kots YM, Syrovegin AM. Fixed sets of invariants of interactions of the muscles of the two joints used in the execution of single voluntary movements. Biofisica 1966;11:1061–6.
[3] Lacquaniti F, Soechting JF. Coordination of arm and wrist motion during a reaching task. J Neurosci 1982;2:399–408.
[4] Morasso P. Spatial control of arm movements. Exp Brain Res 1981;42:223–7.
[5] Morasso P, Mussa Ivaldi FA. Trajectory formation and handwriting: a computational model. Biol Cybern 1982;45(2):131–42.
[6] Morasso P, Mussa Ivaldi FA, Ruggiero C. How a discontinuous mechanism can produce continuous patterns in trajectory formation and handwriting. Acta Psychol 1983;54(1–3):83–98.
[7] Morasso P, Tagliasco V. Analysis of human movements: spatial localisation with multiple perspective views. Med Biol Eng Comput 1983;21:74–82.
[8] Morasso P. Coordination aspects of arm trajectory formation. HMS (Hum Mov Sci) 1993;2:197–210.
[9] Prablanc C, Echellier JF, Komillis K, Jeanerod M. Optimal response of eye and hand motor systems in pointing at a visual target. Biol Cybern 1981;35:113–24.
[10] Rektorys K. Survey of applicable mathematics. Cambridge: MIT Press; 1969.
[11] Teulings HLHM, Thomassen AJWM. Computer aided analysis of handwriting movements. Visible Lang 1979;13(3):218–31.
[12] Viviani P, Terzuolo CA. Space-time invariance in learned motor skills. In: Stelmach GE, editor. Tutorials in motor behaviour. 1980. p. 525–33.
[13] Abend W, Bizzi E, Morasso P. Human arm trajectory formation. Brain 1982;705:331–48.
[14] Hogan N. An organizing principle for a class of voluntary movements. J Neurosci 1984;4:2745–54.
[15] Flash T, Hogan N. The coordination of arm movements: an experimental confirmed mathematical model. J Neurosci 1985;7:1688–703.
[16] Characterization of Smoothness in wrist rotation. 2016http://scholarsarchive.byu.edu/etd/4322/ accessed in 2016.
[17] Opal by APDM, inc. [Online].Available:http://apdm.com/products/movement-monitors/opal/. 2016 accessed in 2016.
[18] Moe-Nilssen R, Helbostad JL. Trunk accelerometry as a measure of balance control during quiet standing. Gait Posture 2002;16(1):60–8. https://doi.org/10.1016/S0966-6362(01)00200-4.
[19] Frosio Iuri, Federico Pedersini N. Alberto borghese autocalibration of MEMS accelerometers. 2016http://ieeexplore.ieee.org/document/4655611/authors accessed in 2016.
[20] Monitoraggio MEMS dell'attività motoria per la valutazione funzionale: validazione di strumenti e riconoscimento preliminare di gesti quotidiani. 2016https://www.politesi.polimi.it/bitstream/10589/2041/3/2010_07_Logica.pdf accessed in 2016.
[21] D'Addio G, Lullo F, Pappone N, Romano M, Iuppariello L, Cesarelli M, Bifulco P. Relationships of kinematics indexes with amplitude and velocity of upper arm reaching movement. IEEE International Symposium on Medical Measurements and Applications, Proceedings 2013. p. 120–3. https://doi.org/10.1109/MeMeA.2013.6549719. 6549719.
[22] Cesarelli M, Iuppariello L, Romano M, Bifulco P, D'Addio G. Bioengineering activities in proprioceptive and robotic rehabilitation at Salvatore Maugeri Foundation. AEIT International Annual Conference 2015. p. 7415277. https://doi.org/10.1109/AEIT.2015.7415277.
[23] Iuppariello L, Romano M, D'Addio G, Bifulco P, Pappone N, Cesarelli M. Comparison of measured and predicted reaching movements with a robotic rehabilitation device. IEEE International Symposium on Medical Measurements and Applications, Proceedings 2014. https://doi.org/10.1109/MeMeA.2014.6860056. 6860056.
[24] Iuppariello L, D'Addio G, Romano M, Bifulco P, Lanzillo B, Pappone N, Cesarelli M. Analysis of reaching movements of upper arm in robot assisted exercises: kinematic assessment of Robot assisted upper arm reaching single-joint movements. Giornale Italiano di Medicina del Lavoro. Ergonomia 2016;38. 2:116–27.
[25] D'Addio G, Lullo F, De Nunzio M, Cesarelli M, Clemente F, Pappone N. Reproducibility of kinematics indexes of upper arm reaching movement in robot assisted therapy. IEEE Symposium on Medical Measurements and Applications, Proceedings. 2012. p. 184–7. 6226663.
[26] D'Addio G, Iuppariello L, Romano M, Lullo F, Pappone N, Cesarelli M. Kinematic indexes' reproducibility of horizontal reaching movements. IFMBE Proceedings 41. 2014. p. 81–4. https://doi.org/10.1007/978-3-319-00846-2_20.

[27] Cesarelli Mario, Bifulco Paolo, Bracale Marcello. Quadriceps muscles activation in anterior knee pain during isokinetic exercise. Med Eng Phys 1999;21(6–7):469–78.
[28] Iuppariello L, Bifulco P, Romano M, D'Addio G, Cesarelli M. A hybrid decomposition method to infer the sub-movements composition of planar reaching movements. Inf Med Unlocked 2017;9:210–8. https://doi.org/10.1016/j.imu.2017.09.004.
[29] Morasso P, Mussa-Ivaldi FA. Trajectory formation and handwriting: a computational model. Biol Cybern 1982;45:131–42.
[30] D'Addio G, Iuppariello L, Gallo F, Bifulco P, Cesarelli M, Lanzillo B. Comparison between clinical and instrumental assessing using Wii Fit system on balance control. IEEE International Symposium on Medical Measurements and Applications, Proceedings 2014. p. 68600124. https://doi.org/10.1109/MeMeA.2014.6860124.
[31] D'Addio G, Iuppariello L, Pagano G, Biancardi A, Lanzillo B, Pappone N, Cesarelli M. New posturographic assessment by means of novel e-textile and wireless socks device. IEEE International Symposium on Medical Measurements and Applications, MeMeA Proceedings 2016. https://doi.org/10.1109/MeMeA.2016.7533798.
[32] Iuppariello L, Bifulco P, D'Addio G, Lanzillo B, Lullo F, Gallo F, Romano M, Cesarelli M. The effects of the vibratory stimulation of the neck muscles for the evaluation of stepping performance in Parkinson's Disease. IEEE International Symposium on Medical Measurements and Applications, MeMeA Proceedings. 2015. p. 606–9. 7145275.
[33] Rohrer B, Fasoli S, Krebs HI, Volpe B, Frontera WR, Stein J, et al. Submovements grow larger, fewer, and more blended during stroke recovery. Mot Contr 2004;8:472–83.
[34] Veer K, Vig R. Identification and classification of upper limb motions using PCA. Biomed Tech (Berl) 2018 Mar 28;63(2):191–6. https://doi.org/10.1515/bmt-2016-0224.
[35] Romano M, Faiella G, Clemente F, Iuppariello L, Bifulco P, Cesarelli M. Analysis of foetal heart rate variability components by means of empirical mode decomposition. IFMBE Proceedings. 57. 2016. p. 71–4.
[36] Mastantuono T, Lapi D, Battiloro L, Cesarelli M, D'Addio G, Iuppariello L, Colantuoni A. Microvascular blood flow regulation impairments in hypertensive obese people. 8th conference of the european study group on cardiovascular oscillations ESGCO 2014. p. 191–2. 6847584.
[37] Romano M, Cesarelli M, Iuppariello L, Faiella G, Bifulco P, D'Addio G. Frequency domain and symbolic dynamics analysis for the study of cardiac pathologies. E-health and bioengineering conference. EHB; 2013. p. 6707269.
[38] Mastantuono T, Muscariello E, Novellino T, Lapi D, Cesarelli M, D'Addio G, Iuppariello L, Colantuoni A. Changes in frequency components of blood flow oscillations in hyperglycemic obese people. 8th Conference of the European Study Group on Cardiovascular Oscillations, ESGCO. 2014. p. 185–6. 6847581.
[39] Kwakkel G, Kollen BJ, Krebs HI. Effects of robot-assisted therapy on upper limb recovery after stroke: a systematic review. Neurorehabilitation Neural Repair 2008;22:111–21.
[40] Veer K, Sharma T. Electromyographic classification of effort in muscle strength assessment. Biomed Tech (Berl) 2018 Mar 28;63(2):131–7. https://doi.org/10.1515/bmt-2016-0038.
[41] Hargrove LJ, Englehart K, Hudgins B. A training strategy to reduce classification degradation due to electrode displacements in pattern recognition based myoelectric control. Biomed Signal Process Control 2008;3(2):175–80. https://doi.org/10.1016/j.bspc.2007.11.005.